Simulation of radial electron dynamics in a Hall effect thruster

IEPC-2019-593

Presented at the 36th International Electric Propulsion Conference
University of Vienna, Austria
September 15-20, 2019

A. Marín-Cebrián*, A. Domínguez-Vázquez†, P. Fajardo‡ and E. Ahedo§
Equipo de Propulsión Espacial y Plasmas, Universidad Carlos III de Madrid, Spain

A new algorithm for simulating the effect of an axial source of particles is implemented in a 1D radial particle-in-cell model of an annular Hall effect thruster discharge with secondary electron emission from the walls. New particles are generated into the domain from a prescribed axial source with a self-adjusted injection frequency so that a sustained discharge featuring a given plasma and neutral density is ensured. The new algorithm extends the model capabilities incorporating information of the electron population from the axial direction, which is external to the radial model and essential for determining the the discharge structure, and allows to simulate a more complete discharge scenario in which the ionization and the contribution of the axial plasma flows compensate the plasma wall losses and recombination in the thruster acceleration region. The new algorithm performance is analyzed and a preliminary parametric study is presented.

I. Introduction

The Hall effect thruster (HET) is already a mature technology, used in a wide range of space missions. Despite this success, there are still open problems hindering its optimization and affecting its performance. One of them is related to the plasma-wall interaction, which is responsible for plasma recombination, energy losses and wall erosion. Moreover, the low collisionality of the discharge and the secondary electron emission (SEE) from the thruster walls are responsible for the departure of the electron velocity distribution function (VDF) from a Maxwellian one. Previous studies[1–3] with particle-in-cell (PIC)/Monte Carlo Collision (MCC) formulations[4–6] in a 1D planar (1Dp) scenario, analyzed the electron VDF for different values of the axial electric field, collisional frequencies, and SEE yields from the walls.

Three recent papers by our group 7–9 have developed a 1D radial (1Dr) PIC/MCC model of an annular HET plasma discharge, based on a previous one by Taccogna.[10–12] In references 7–9, it was discussed that in such a low-dimensional model, there exists a certain arbitrariness on setting some important plasma parameters. In particular, there is a non-trivial relation between the plasma and neutral density to achieve a sustained discharge. One of the most relevant improvements presented in Ref. 7 corresponds to an ionization-controlled discharge (ICD) algorithm that assures a stationary discharge featuring a prescribed mean plasma density without the need of an a contribution of axial plasma flows. By self-adjusting the background neutral density, the plasma generated through ionization adjusts exactly the plasma-wall losses, resulting in a steady state plasma response.

In this work, we extend that ionization controlled model by adding the effects of axial plasma flows. A new axially controlled discharge (ACD) algorithm which simulates an axial source of particles is presented. This algorithm extends the code capabilities by: (*i*) allowing to simulate a sustained discharge with prescribed plasma and neutral densities, (*ii*) reproducing a wider range of scenarios in which the neutral gas ionization and the contribution from the axial plasma flows compensate the plasma-wall losses and recombination in

*Master student, 100329589@alumnos.uc3m.es
†PhD candidate, addoming@ing.uc3m.es.
‡Associate Professor, pfajardo@ing.uc3m.es
§Professor, eduardo.ahedo@uc3m.es

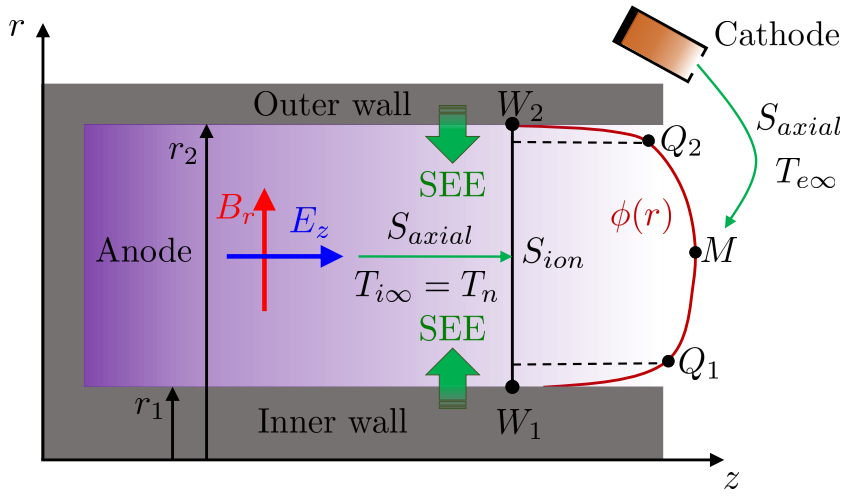

Figure 1. Sketch of the domain under study inside the HET

the HET acceleration region, and (*iii*) incorporating information from the plasma axial transport into the radial dynamics.

The paper is structured as follows. The main physical aspects of the model are summarized in Sec. II. The simulation results are presented and discussed in Sec. III. Finally, conclusions are drawn in Sec. IV.

II. The radial model

The complete description of the radial model can be found in Refs. 7 and 9, and it is here briefly outlined. The 1Dr model simulates the plasma radial structure at a given location near the exit of the acceleration region of a HET chamber. The different species taken into account are: electrons e, singly-charged ions i and neutrals n. The latter are modelled as a background spatially homogeneous population with density n_n and a constant temperature T_n. Electrons and ions are modelled as two populations of macroparticles with time-evolving densities and temperatures, n_j and T_j ($j = i, e$), respectively. Every simulated macroparticle features the same macroparticle weight W, or number of elementary particles, which remains constant throughout the simulation.

The divergent-free radial magnetic field is

$$B_r(r) = B_{r1}\frac{r_1}{r}, \tag{1}$$

with B_{r1} known at r_1 (r_1 and r_2 are the inner and outer radii as it can be seen in Fig. 1). A constant and uniform axial electric field E_z is prescribed in the 1Dr model, which provides the $\boldsymbol{E} \times \boldsymbol{B}$ azimuthal drift motion on the magnetized electron population. The ions' secular E_z acceleration is ignored; ions are inserted initially or created later with a prescribed axial fluid velocity u_{zi} instead, thus avoiding ion particle refreshing. On the other hand, both ions and electrons are accelerated by the radial electric field $E_r = -d\phi/dr$ obtained by solving Poisson equation along the radial direction.

Regarding plasma-wall interaction, ions and electrons reaching the radial walls are collected and thus eliminated from the simulation domain. Ion recombination is not explicitly simulated. The SEE produced by impacting electrons on the wall follows the probabilistic law presented in Ref. 13. In this work, only true secondary (TS) electrons are considered, which feature a semi-Maxwellian emission from the thruster walls with an average emission energy T_{eW}.

The treatment of collisions between different populations and the applied MCC algorithms can be found in Ref. 7. Electron-neutral collisions (including elastic, excitation and ionization ones) and Coulomb collisions are simulated. Secondary electrons are transferred to the primary population when they undergo a collision with neutrals or a large angle (higher than 90 degrees) Coulomb collision. For the sake of facilitating the analysis of the plasma discharge response, three different electron species are considered hereafter: primary electrons p, and secondary electrons emitted by the inner $s1$, and outer $s2$ walls (see Fig. 1).

A. The discharge control algorithm

The aim here is to simulate a quasi-stationary discharge with a prescribed mean plasma density, that is $\bar{n}_e(t) \approx \text{const} = n_{e0}$. In a 1D model, this requires to take some decisions on the behavior of the particle sources and sinks. In 1D cylindrical geometry, the conservation equations for ions and electrons reduce to

$$\frac{\partial n_j}{\partial t} + \frac{1}{r}\frac{\partial}{\partial r}(r n_j u_{rj}) = S_{ion} + S_{axial,j}, \qquad j = i, e, \tag{2}$$

where: $n_j u_{rj}$ is the species radial flux; the ionization source term is

$$S_{ion,e} = n_e \nu_{ion}^{en}, \qquad \nu_{ion}^{en} = n_n R_{ion}(T_e), \tag{3}$$

with $R_{ion}(Te)$ the ionization rate and ν_{ion}^{en} the ionization frequency; and $S_{axial,j}$ is the source term due to the net axial contribution for species j. In a 2D (r, z) model one would have $S_{axial,j} = \partial(n_j u_{zj})/\partial z$, but, here $S_{axial,j}$ is as arbitrary as the HET radial section we are attempting to simulate.

In the quasi-steady state, the integral of the continuity equation in Eq. (2) over the plasma volume (expressed in electric current units) yields

$$I_{wall,j} \approx I_{ion} + I_{axial,j}, \qquad j = i, e, \tag{4}$$

with $I_{wall,j}$ the species current lost into the wall, I_{ion} the (equivalent) current created through volumetric ionization, and $I_{axial,j}$ the current injected (or extracted) through the axial flow. While $I_{wall,j}(t)$ is obtained directly from the dynamic plasma response, both I_{ion} and $I_{axial,j}$ depend on the particular model formulation. Thus, we can distinguish between *axially-controlled* and *ionization-controlled* discharges depending on whether $I_{axial,j}$ is much larger or much smaller than I_{ioniz}, respectively.

The ionization dominated model[10] assumed that $S_{axial,e} = S_{axial,i} = 0$. It was then demonstrated[7] that this model could not assure a sustained discharge if both n_n and $\bar{n}_e$ were fixed at the same time. In the proposed ICD model, the average plasma density, $\bar{n}_e$, was chosen as the target value to be conserved throughout the simulation while $n_n(t)$ is adjusted in order to satisfy $I_{ioniz} \approx I_{wall,j}$.[7]

In the new ACD algorithm presented here, both n_n and $\bar{n}_e$ are known (and constant) and we attempt to achieve a sustained discharge by adding plasma from a virtual axial source representing the differential flux $\partial(n_j u_{zj})/\partial z$. Electrons and ions are introduced in the same amount to avoid introducing net charge in the domain, which would perturb the system state. The ACD algorithm defines

$$S_{axial,j} = \bar{n}_e \nu_{axial} \qquad j = i, e, \tag{5}$$

where ν_{axial} stands for the axial source frequency, which is regulated, in order to maintain the desired plasma density. The temporal ACD regulation law is

$$\nu_{axial}^{(k)} = \frac{n_{e0}}{\bar{n}_e^{(k)}}\, \nu_{axial}^{(k-1)}, \tag{6}$$

where (k) is the current PIC timestep and $(k-1)$ the previous one.

The injected electrons and ions are homogeneously distributed inside the bulk plasma region; sheaths are excluded to avoid introducing very energetic electrons close to the walls that will increase artificially the SEE. The new electrons are introduced in the domain following a Maxwellian distribution at a given temperature $T_{e,ax}$. We proceed similarly with injected ions taking for them a temperature equal to the neutral background ($T_{i,ax} = T_n$).

Thus, the new algorithm allows to reach a quasi-stationary regime in three scenarios: (i) if ionization is switched off or not playing an important role, all the contribution to compensate the losses to the walls will come from the axial source; (ii) if the ionization is active and comparable to the contribution of the axial source term, we will have a mixed regime in which both terms (ionization and axial) will have a contribution; (iii) if ionization on its own is capable of sustaining the discharge the axial source contribution will vanish, being the ionization production the one in charge of reaching the desired final state.

III. Simulations

The simulations shown in this paper are the result of a work in progress in which we try to get a deeper insight into the radial electron dynamics and how they are affected by the axially injected particles from the new discharge control algorithm.

The settings for the reference case simulation are included in Sec. III.A. Section III.B is devoted to the discussion of the results, which are divided in two parts: validation of the new algorithm (Sec. III.B.1) and a small parametric study changing the most relevant parameters affecting the steady-state electron temperature (Sec. III.B.2).

A. Simulation settings

For all the simulations, xenon was considered as the HET propellant and the extended discharge control algorithm was used to achieve a sustained discharge. In order to discuss just a planar scenario within the cylindrical code, the radius r is displaced artificially 1000 m. Under these conditions, cylindrical expansion effects (i.e. terms $\sim 1/r$) vanish[7] and the imposed magnetic field is approximately constant ($B_{r2}/B_{r1} = r_1/r_2 \simeq 1$). Thus, the magnetic mirror effect and the asymmetries found in a typical cylindrical case become negligible, making easier to understand and interpret the results. Table 1 summarizes the main input parameters for the reference case (Case 1) of this work. A brief description of all simulated cases is:

- **Case 1** is chosen as the reference case. The simulation settings were set such that it reproduces similar conditions to those studied in Case 5 of Ref. 9 using the ICD algorithm.
- **Case 2** studies the influence of increasing the temperature at which electrons are injected in the domain keeping the electric field and background neutral density equal to Case 1. In this case, the electrons are introduced at a temperature of 20 eV, which is representative of the exit region of a HET discharge.
- **Case 3** analyzes the effects of reducing the background density by one order of magnitude compared to Case 2.
- **Case 4** discusses the consequences of having a twice stronger axial electric field than Case 3.

The weight of the macroparticle (W) has been chosen such that the initial populations of electrons and ions are $N_{p0} \approx 10^5$. This number corresponds to approximately 70 macroparticles per cell. A larger number of particles per cell would reduce the noise in the results, but would not change the trends observed.

B. Results

The simulations are started with full Maxwellian distributions for the electron and ion populations with identical particle densities. Due to the high mobility of electrons at the initial timesteps, many of them reach the HET walls, charging them negatively. The build up of negative surface charges there creates the Debye sheaths that confine the electrons away from the walls. From that time on, for an electron to reach the wall it is required that it has an energy in the radial direction greater than the required to cross the potential drop of the sheaths. Therefore, only the fastest electrons are able to impact the walls. The discharge control algorithm starts acting after the sheaths are fully developed to avoid perturbing the radial dynamics initial transient.

1. Validation

The first objective is validating that the new algorithm is capable of controlling the mean electron density $\bar{n}_e$, thus, achieving a sustained discharge. For that purpose the time evolution of some relevant variables in the reference case simulation is plotted in Fig. 2.

From Fig. 2(a) it can be noted that initially, the electron density drops until the sheaths are formed and the discharge control algorithm starts introducing particles. After approximately 2 μs the mean electron density stabilizes around its target value and oscillates slightly up and down that point until the end of the simulation.

The electron sources that compensate the losses to the HET walls are the ionization production and the axial injection term. Fig. 2(b) depicts how the production frequency of these two sources changes during the simulation time. It is worth mentioning that both of them are tightly related since one affects to the other directly. If ionization production is almost enough to achieve a sustained discharge, there will be practically no need to introduce "axial" particles. For lower ionization, electrons and ions are injected "axially". In particular the new "axial" electrons modify the electron temperature (T_e), which in turn affects ionization, as it can be noted from Eq. (3).

Type	Description, symbol and units	Case 1
Populations settings	Number of elementary particles per macroparticle, W (-)	$7.06 \cdot 10^{13}$
	Initial average plasma density, n_{e0} ($10^{17}\mathrm{m}^{-3}$)	0.8
	Initial number of ions and electrons macroparticles*, N_{p0} (-)	106814
	Initial electron temperature, T_{e0} (eV)	10
	Initial ion temperature, T_{i0} (eV)	1
	Ion axial mean velocity, u_{zi} (km/s)	10
	Background neutral density, n_{n0} (10^{17} m^{-3})	40
	Neutral temperature, T_n (K)	700
E, B fields	Electric field axial component, E_z (V/cm)	100
	Magnetic field radial component at inner radius, B_{r_1} (G)	124.84
Simulation parameters	Non-true-secondary emission	OFF
	True-secondary emission	ON
	Average true-secondary electrons emission energy, T_{eW} (eV)	2
	Inner radius, r_1 (cm)	$10^5 + 3.5$
	Outer radius, r_2 (cm)	$10^5 + 5.0$
	Number of nodes, N_r (-)	1500
	Grid spacing*, Δr (μm)	10
	Timestep, Δt, (ps)	5
	Initial axial source frequency, ν_{axial} (kHz)	1
	Axially injected electron temperature, $T_{e,ax}$ (eV)	6.9
Physical parameters	Debye length*, λ_D (μm)	83.1
	Electron Larmor radius*, r_l (μm)	963.7
	Inverse of plasma frequency*, $1/\omega_{pe}$ (ps)	62.7
	Inverse of electron cyclotron frequency*, $1/\omega_{ce}$, (ps)	455.5

Table 1. Main input parameters including initial population settings, externally applied fields and grid definition for Case 1 (reference case for this paper due to similarities with Domínguez-Vázquez *et al.*[9] Case 5). The magnitudes marked with an asterisk (*) are not input parameters of the model, but are derived from the other parameters instead. The variables named as physical parameters are estimated from the other input values given at initial conditions.

Therefore, axial injection and production from ionization are highly coupled processes. As shown in Fig. 2(a), the control algorithm through the injection of axial particles is able to reach an equilibrium but there is a constant need for correction in order not to move away from this operational point.

In particular, for Case 1, it can be observed from Fig. 2(b) that none of the two contributions to the mass balance (ionization and axial injection) is clearly dominant, the ionization contribution being slightly higher.

2. Parametric study

Fig. 3 shows the radial profiles of the main parameters of interest in this study for the primary and secondary electron population averaged over the last microsecond of the simulation. For all the cases W_1, W_2 and M indicate the position of the inner and outer walls, and the channel mid-radius, respectively. The vertical

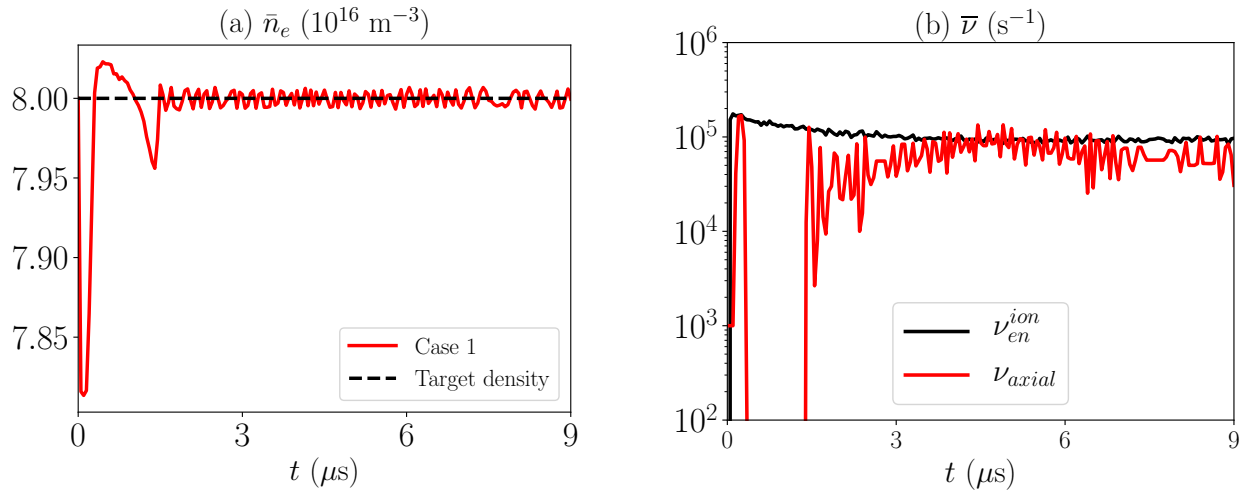

Figure 2. Time evolution of (a) the average electron density in the simulation domain with respect to the target value; (b) electron production sources contribution.

dashed lines in the plots represent the approximate edges of the Debye sheaths, which correspond to points Q_1 and Q_2. The radial VDFs at points M and Q_1 for the primary electron population are depicted in Fig. 4. Table 2 summarizes relevant plasma parameters for the 4 cases considered.

Case 1 settings were selected such that they represent similar conditions to those of Case 5 of Ref. 9, so as to prove the validity of the new algorithm. In this low-collisional regime, Coulomb collisions are negligible compared with electron-neutral collisions, being the elastic e-n collisions clearly dominant. Comparing the primary and secondary electron population densities from Figs. 3(c) and (d), it can be observed that secondary electrons are several orders of magnitude less numerous than primary ones. Therefore, SEE has a minor effect when shaping the electric potential distribution. Moreover, the electric current densities to the walls are also dominated by the much more populated primary electrons. Regarding the VDFs shape, the high energy tail depletion observed by Domínguez-Vázquez *et al.*[7,9] can be clearly found in Fig. 4(b). These tails are only partially refilled with high velocity electrons by infrequent collision events. Secondary electrons bounce between the sheaths until they get transferred to the primary population through large-angle Coulomb collisions or collisions with the neutral gas background. The radial temperature component (parallel to the magnetic field) comes determined by radial dispersion of velocities while the perpendicular plane temperature can be associated to the electron gyromotion. Figure 3 confirms that, as expected, no radial asymmetries exist. Plot 3(b) show that electrons inside the sheaths are faster, which explains the density drop inside the sheaths.

Comparing Case 1 and 2, the influence of the axially injected electron temperature can be studied. For Case 2 this temperature has been increased from 6.9 to 20 eV (which is closer to the temperature of a typical HET discharge) while keeping all the other simulation parameters fixed. At steady-state, similar potential curves and density profiles are obtained [see Fig. 3(a)]. The electric potential change towards slightly higher values can be attributed to the more energetic injected particles. The SEE increases too but the n_{s1} profile shown in Fig. 3(d) is still far below the primary electron density depicted in Fig. 3(c). Figures 3(e) and 3(f) reveal that B-parallel and B-perpendicular primary electron temperature components are increased simultaneously. Therefore, as shown in Fig. 3(h), the steady-state total temperature of the primary electron population is higher than that of Case 1, which confirms that increasing the temperature of the axial source $T_{e,ax}$ results in higher primary electron temperatures in the domain. As can be drawn from the inspection of the radial profiles of the temperature anisotropy ratio $T_{\|p}/T_{\perp p}$ shown in Fig. 3(g), Case 2 presents a slightly more anisotropic primary electron population with respect to the Case 1.

Moving from Case 2 to Case 3 means reducing the neutral background density one order of magnitude. This implies that the e-n collisions are reduced in frequency almost proportionally to that reduction in neutral density, as it can be seen in Table 2. Thus, in this regime, ionization and excitation collisions become rare events that happen with even smaller frequency than Coulomb collisions. Since ionization practically does not contribute to the mass balance generating new electrons, the discharge is mainly sustained by the axially

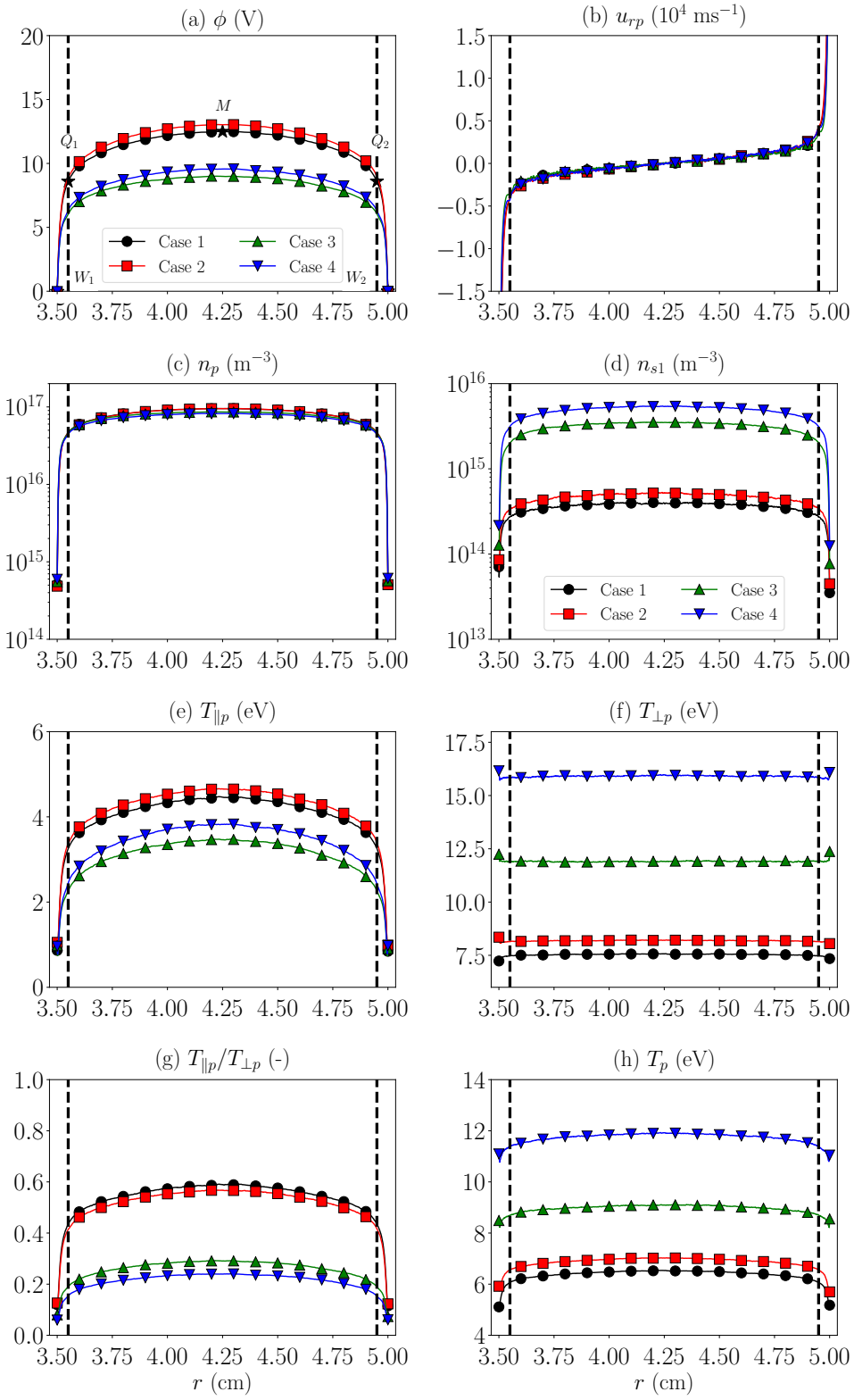

Figure 3. Time-averaged (over the last microsencond of simulation) radial profiles of macroscopic magnitudes for the primary electron population: (a) electric potential profile, (b) radial electron velocity, (c) primary electron density, (d) density of the secondary electrons emitted from the inner wall (similar results are obtained for those emitted from the outer wall, and are thus omitted), (e) B-parallel temperature (corresponding to the radial direction), (f) B-perpendicular temperature, (g) parallel-to-perpendicular temperature ratio and (h) total temperature. The black stars on (a) indicate the location of the walls (W_1 and W_2), sheath edge (Q_1 and Q_2) and the mid-radius position (M).

Type and units	Description and symbol	Case 1	Case 2	Case 3	Case 4
Axial electron temperature (eV)	Axial temperature $T_{e,ax}$*	6.9	20	20	20
Neutral density (10^{17} m^{-3})	Background neutral density n_n*	40	40	4	4
Axial electric field (V/cm)	Imposed electric field in z E_z*	100	100	100	200
Electric potentials (V)	At the mid radius M, ϕ_M	12.50	13.03	8.99	9.57
	At the inner sheath edge Q_1, ϕ_{Q_1}	8.60	8.89	6.03	6.33
	At the outer sheath edge Q_2, ϕ_{Q_2}	8.60	8.95	6.06	6.29
	At the inner wall W_1, ϕ_{W_1}	−0.03	−0.05	−0.03	−0.03
	At the outer wall W_2, ϕ_{W_2}	0.00	0.00	0.00	0.00
Current densities (A/m^2)	p to the inner wall, $\lvert j_{p,1-}\rvert$	17.16	17.89	15.99	18.21
	$s1$ to the inner wall, $\lvert j_{s1,1-}\rvert$	0.22	0.31	0.68	1.31
	$s1$ from the inner wall, $\lvert j_{s1,1+}\rvert$	4.18	4.97	6.13	5.24
	$s2$ to the inner wall, $\lvert j_{s2,1-}\rvert$	1.69	2.02	3.08	10.40
	p to the outer wall, $\lvert j_{p,2+}\rvert$	16.98	17.84	16.18	18.56
	$s1$ to the outer wall, $\lvert j_{s1,2+}\rvert$	1.82	2.08	2.94	5.09
	$s2$ to the outer wall, $\lvert j_{s2,2+}\rvert$	0.21	0.28	0.66	1.27
	$s2$ from the outer wall, $\lvert j_{s2,2-}\rvert$	3.95	4.80	6.18	10.52
Electron temperatures at M (eV)	p parallel, $T_{\parallel p,M}$	4.46	4.65	3.46	3.82
	p perpendicular, $T_{\perp p,M}$	7.57	8.21	11.91	15.97
	p total, $T_{p,M}$	6.53	7.02	9.09	11.92
Collision frequencies (MHz)	e-n elastic collision, ν_{en}^{el}	2.141	2.142	0.204	0.200
	e-n excitation collision, ν_{en}^{ex}	0.116	0.125	0.014	0.025
	e-n ionization collision, ν_{en}^{ion}	0.094	0.107	0.015	0.031
	e-i Coulomb collision, ν_{ei}^{Coul}	0.072	0.073	0.066	0.037
	e-e Coulomb collision, ν_{ee}^{Coul}	0.020	0.018	0.023	0.014
	i-i Coulomb collision, ν_{ii}^{Coul}	0.089	0.092	0.084	0.088
Axial injection frequency (MHz)	Axial source frequency, ν_{axial}	0.060	0.054	0.127	0.167
Production frequency ratio (-)	$\nu_{axial}/\nu_{en}^{ion}$	0.64	0.50	8.47	5.39

Table 2. Main parameters characterizing the steady-state discharge for the different cases considered. Time-averaged values over the last μs of simulation time are considered. The magnitudes marked with an asterisk (*) are input parameters.

injected electrons generated by the ACD. In this simulation the axial injection frequency and the e-n elastic collisions have the same order of magnitude. As a consequence of this drastic decrease in collision events, it was expected that the radial velocity becomes more uniform, and therefore, a much lower radial temperature can be observed [see Fig. 3(e)]. This temperature reduction can also be clearly observed in Fig. 4, where it can be noted that the VDF for Case 3 is significantly narrower than for Case 2. Taking into consideration that the electrons trying to reach the wall are less energetic than in Cases 1 and 2, the required potential to confine the electrons is lower. As shown in Fig. 3(d), the secondary electron population increases by a factor of 6 due the aforementioned reduction in collisions (collisions with neutrals was the main mechanism by which secondary electrons got transferred to the primary population in Cases 1 and 2; then, because the neutral density is reduced 10 times, the rate at which secondary electrons become primary ones decreases remarkably). Nevertheless, they are still far less numerous than primary electrons and do not play an important role in shaping the electric potential. Again, due to this lack of collisions, the energy stored in the B-perpendicular plane does not get transferred to the radial (i.e. B-parallel) direction, as long as the highly

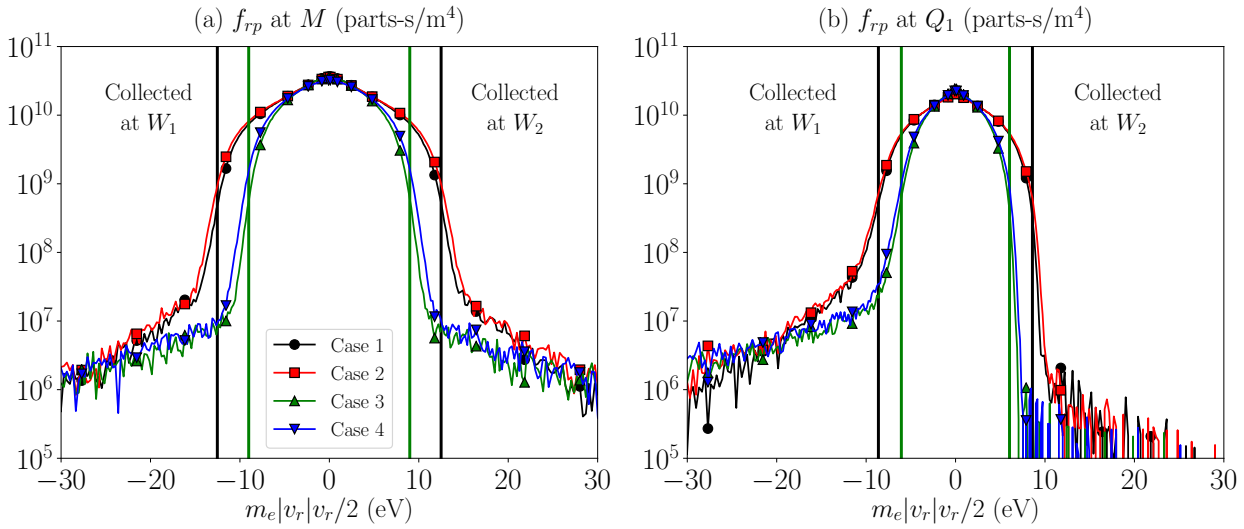

Figure 4. Steady-state radial primary electron VDFs: (a) at M and (b) at Q_1.

energetic electrons moving in the perpendicular plane rarely undergo a collision that changes the direction of their motion towards the radial direction. The resulting B-perpendicular temperature that can be observed in Fig. 3(f) is mainly determined by the temperature of the initial population and the axially introduced particles. It is worth mentioning that the perpendicular temperature is higher than that of the two previous cases. This combination of reducing the radial temperature and increasing the perpendicular temperature makes the electron population greatly anisotropic [see Fig. 3(g)]. The aforementioned changes have the net effect of increasing the total temperature of the primary electrons.

Finally Case 3 is compared to Case 4, in which the axial electric field has been doubled in strength to analyze the effect of this parameter on the plasma dynamics. From Figs. 3(a) and 3(c) it can be noted that this change in E_z does not have much influence on the radial potential or the primary electron density. The radial temperature increases marginally because of the fact that there is more energy in the system. Then, as the electrons impacting with the walls are more energetic the SEE is higher than in Case 3, and so the secondary electrons density [see Fig. 3(d)]. Most of the energy stored in the domain is allocated in the perpendicular plane similarly to what could be observed for Case 3 and, in Fig. 3(f), it can be clearly observed the effect of doubling E_z on the perpendicular temperature. Anisotropy increases [see Fig. 3(g)] with respect to Case 3 but not significantly and the total temperature rises [refer to Fig. 3(h)].

A relevant question is what, in this radial model, determines the mean electron temperature (which, for the present simulations with low secondary electron density, can be assimilated to T_p). In the sustained discharge this temperature is set by the steady-state energy balance, which can be expressed as

$$P_{sinks} = P_{sources}, \qquad P_{sinks} \simeq P_{ion} + P_{ex} + P_{wall,t}, \qquad P_{sources} \simeq P_{elec} + P_{wall,f} + P_{axial}, \tag{7}$$

where: P_{ion} and P_{ex} denote the losses due to ionization and excitation collisions; $P_{wall,t}$ stands for the electron energy losses to the HET walls; $P_{wall,f}$ is the energy gain from electron emission by the walls (negligible for low T_{eW}); P_{elec} is the energy transmitted to the electrons by the work of the electric field; and P_{axial} is the energy injected "axially".

Considering a prescribed average plasma density in the domain $\bar{n}_e$, the energy loss due to inelastic collisions (ionization and excitation) depends mainly on n_n and T_e. The losses to the walls are more difficult to characterize but, for sure, they depend on T_e and E_z (this last one through the $\boldsymbol{E} \times \boldsymbol{B}$ azimuthal electron energy). P_{elec} has axial and radial contributions, which depend at least on E_z and T_e. Finally, P_{axial} depend on $T_{e,ax}$ and indirectly on n_n. Therefore, we can infer that T_e is an implicit function of several parameters, which must be analyzed still.

IV. Summary and conclusions

The aim of this work was to present the new ACD algorithm, capable of enabling the simulation of a sustained discharge through axial addition of plasma. It extends the previous model capabilities allowing to simulate a more general discharge scenario, in which both contributions, ionization and axial particle flows, balance the plasma losses to the walls. The injection frequency from the axial source is adjusted to maintain constant the average electron density in the domain throughout the simulation. New particles are generated in the domain, sampling them from a Maxwellian distribution at a given temperature (electrons are generated with a prescribed axial injection temperature while ions share the same temperature as the neutral background).

A preliminary parametric analysis was done changing relevant parameters affecting the steady-state electron temperature. The effects studied were: different axial injection temperature (Cases 1 and 2), background neutral density reduction (Cases 2 and 3) and axial electric field strength (Cases 3 and 4). From Cases 1 and 2 it was concluded that, under the regime in which axial injection is not dominant over ionization, the rise (from 6.9 eV to 20 eV) in axial injection electron temperature does not affect significantly the results obtained. Nevertheless, it confirmed that increasing the axial injection electron temperature yields a higher overall electron temperature in the domain. In Cases 2 and 3 the neutral density is reduced by one order of magnitude and, therefore, electron-neutral collisions are proportionally reduced. Under this regime axial injection becomes dominant and the effect of ionization is minor. The drastic reduction in collisions affects: (*i*) the radial temperature, which is determined by the dispersion in radial velocities mainly due to elastic collisions with neutrals; (*ii*) the number of secondary electrons in the domain, since the main mechanism through which secondary electrons get transferred to the primary population is collisions; and (*iii*) the temperature anisotropy ratio, because in this low-collisional plasma discharge the energy stored in the perpendicular direction rarely gets transferred to the radial direction. Comparing Cases 3 and 4 it can be observed that there are no substantial changes in the electric potential or the primary electron density, which indicates that, although the SEE is higher, it is not dominant. The problem becomes slightly more anisotropic because the energy in the perpendicular plane increases with the axial electric field but the radial temperature does not feel that change so much.

It can be concluded that the new discharge control algorithm is capable of achieving a sustained HET discharge under a wide range of initial conditions. Nevertheless, it has been proven that the temperature in the domain cannot be controlled only by adding an axial source of particles since there are other parameters that also have a great influence on the final electron temperature (most notably the background neutral density, the axial electric field and the secondary electron emission from the thruster dielectric walls). The energy balance equation is the implicit relationship determining the steady-state electron temperature as a function of, at least, the axial electric field, the background neutral density and the axially injected electron temperature, for a given average plasma density in the domain. Further work should elucidate more quantitatively that relationship.

The development of the ACD algorithm must help to analyze in future work cases where the SEE yield approaches 100% and secondary electrons become more dominant in the discharge. Preliminary studies have shown that the ICD algorithm is not appropriate to deal with those situations. Finally, the ACD algorithm needs to be extended to consider situations where ionization is too strong and there must be an axial sink of particles to sustain the discharge. This case poses the problem of selecting the particles to be taken away.

V. Acknowledgements

This work has been supported by the PROMETEO-CM project, Grant number Y2018/NMT-4750 (Comunidad de Madrid/FEDER/FSE) and Project ESP2016-75887 (Spain's National Research and Development Plan - MINECO/ FEDER).

References

[1]D. Sydorenko, A. Smolyakov, I. Kaganovich, and Y. Raitses. Kinetic simulation of secondary electron emission effects in Hall thrusters. *Physics of Plasmas*, 13(1):014501, 2006.

[2]D. Sydorenko, A. Smolyakov, I. Kaganovich, and Y. Raitses. Modification of electron velocity distribution in bounded plasmas by secondary electron emission. *Plasma Science, IEEE Transactions on*, 34(3):815–824, 2006.

[3]I. D. Kaganovich, Y. Raitses, D. Sydorenko, and A. Smolyakov. Kinetic effects in a Hall thruster discharge. *Physics of*

Plasmas, 14(5):057104, 2007.

[4]C. K. Birdsall and A. B. Langdon. *Plasma physics via computer simulation.* Adam Hilger, Bristol, Philadelphia and New York, 1991.

[5]C. K. Birdsall. Particle-in-Cell charged particle simulations, plus Monte Carlo collisions with neutral atoms, PIC-MCC. *Trans. Plasma Sci.*, 19(2):65–85, 1991.

[6]R. W. Hockney and J. W. Eastwood. *Computer simulations using particles.* Adam Hilger, Bristol and New York, 1988.

[7]A. Domínguez-Vázquez, F. Taccogna, and E. Ahedo. Particle modeling of radial electron dynamics in a controlled discharge on a Hall thruster. *Plasma Sources Science and Technology*, 27(6):064006, 2018.

[8]A. Domínguez-Vázquez, F. Taccogna, P. Fajardo, and E. Ahedo. Influence of relevant parameters on the radial PIC simulation of a Hall effect thruster discharge. In *Space Propulsion Conference*, paper SP2018-288, Seville, Spain, May 14-18, 2018. 3AF, https://www.3af.fr/.

[9]A. Domínguez-Vázquez, F. Taccogna, E. Ahedo, and P. Fajardo. Parametric study of the radial plasma-wall interaction in a Hall thruster. *Journal of Physics D: Applied Physics*, 52(47):474003, 2019.

[10]F. Taccogna, S. Longo, M. Capitelli, and R. Schneider. Particle-in-cell simulation of stationary plasma thruster. *Contributions to Plasma Physics*, 47(8-9):635–656, 2007.

[11]F. Taccogna, S. Longo, M. Capitelli, and R. Schneider. Surface-driven asymmetry and instability in the acceleration region of a Hall thruster. *Contrib. Plasma Phys.*, 48(4):1–12, 2008.

[12]F. Taccogna, R. Schneider, S. Longo, and M. Capitelli. Kinetic simulations of a plasma thruster. *Plasma Sources Sci. Technol.*, 17(2):024003, 2008.

[13]M. A. Furman and M. T. F. Pivi. Probabilistic model for the simulation of secondary electron emission. *Phys. Rev ST Accel. Beams*, 5(12):124404, 2002.